Error Performance of Information Decoder for SWIPT With Integrated Receiver

Erica Debels, *Graduate Student Member, IEEE*, and Marc Moeneclaey, *Fellow, IEEE*

***Abstract*— Simultaneous wireless information and power transfer can be realized by means of an *integrated* receiver, where both the energy harvester and the information decoder operate on the rectified received signal. We investigate the effect of the non-linearity of the rectifier on the error performance of the information decoder when transmitting over a Nakagami-m fading channel. Through analysis and simulation, we demonstrate that the low-noise error performance strongly depends on the small-signal behavior of the rectifier, even when the average operating point is outside the small-signal area. Approximating for analysis purposes the rectifier by a quadratic detector yields accurate bit error rate results for the fading channel in the low-noise regime, whereas an over-optimistic error performance is obtained when applying the envelope detector approximation.**

***Index Terms*— SWIPT, integrated receiver.**

I. Introduction

SIMULTANEOUS wireless information and power transfer (SWIPT) is a promising technique for powering energy-limited information-processing devices, which are commonly used in the Internet of Things. The concept of SWIPT was first proposed in [1], where it is assumed that the receiver is able to extract information and power from the same signal, at the same time. Later, SWIPT has mainly been studied in the context of a separated receiver (RX) (see [2]–[4] and the references therein). Here, the RX for energy harvesting (EH) and the RX for information decoding (ID) use a different antenna, or share an antenna by operating either in time-switching or power-splitting mode. The EH-RX contains a rectifier, whereas the ID-RX uses a mixer and oscillator to convert the RF signal to baseband.

In [5] a novel type of RX was proposed, namely the integrated information and energy receiver (IIE-RX). The IIE-RX rectifies the incoming signal, and the rectifier output current is subsequently split between the EH and ID circuits. Because of the dual use of the rectifier, neither mixer nor oscillator are required. Compared to the separated RX, the IIE-RX enjoys a reduction of implementation complexity and power consumption, and exhibits a more favorable EH-ID trade-off [4], [5].

Most often, a simple rectifier circuit, consisting of a diode followed by an RC lowpass filter, is used [5]–[13]. In [6], this rectifier is approximated by an envelope detector (ED) for analysis purposes. Assuming low power at the rectifier input, a quadratic detector (QD) approximation of the rectifier characteristic is used in [5], [7]–[10]. This approximation results from truncating the Taylor series expansion of the diode current-voltage characteristic. In [11], the accuracy of the truncated Taylor series is improved by including terms beyond the second order. No approximation of the diode current-voltage characteristic is introduced in [12], [13].

The performance of the IIE-RX has been studied by several authors for different scenarios. In the case of a single-input single-output (SISO) AWGN channel, an ED and a QD have been considered in [6] and [5], respectively. Assuming a SISO Rayleigh fading channel and a QD, [8] investigated the error performance of non-coherent detection in the absence of channel state information. The performance of the IIE-RX involving a multi-antenna TX with linear precoding has been investigated assuming a QD and both Rayleigh and Rician fading in [7] and considering the actual rectifier characteristic and Rayleigh fading in [13].

In this letter, we investigate the error performance of the ID in the IIE-RX, using biased ASK [6] on a SISO Nakagami-m [15] block-fading channel, with the receiver knowing (e.g., through estimation from pilot symbols) the distorted ASK constellation at the rectifier output. Our main contribution is the derivation of an analytical expression for the bit error rate (BER) of the maximum-likelihood (ML) detector in the low-noise regime. We do this for an actual rectifier characteristic and for both the ED en QD approximations. Through analysis and simulation, we show that (i) the QD provides a very good approximation of the low-noise BER of the actual rectifier, even when the average operating point is outside the quadratic region of the rectifier characteristic; and (ii) the BER resulting from the ED turns out to be much below the BER of the actual rectifier. This contrasts with the harvested power of the rectifier, which is similar to that of the QD or the ED, when the average operating point is in the quadratic region or the linear region, respectively. Compared to [5]–[13], we consider more general channel and/or rectifier models.

II. SWIPT With Integrated ID and EH Receiver

We consider a single-antenna TX sending symbols $a(k)$ from a normalized constellation (i.e., $\mathbb{E}[|a(k)|^2] = 1$) over a flat Nakagami-m block-fading channel to a single-antenna IIE-RX. The IIE-RX rectifies the incoming signal, after which the current is split between the ID and the EH. The corresponding block diagram is shown in Fig. 1, with the main symbols listed in Table I.

Manuscript received November 4, 2020; revised December 3, 2020; accepted December 17, 2020. Date of publication December 21, 2020; date of current version April 9, 2021. This research work was carried out in the frame of Fonds de la Recherche Scientifique - FNRS and Fonds Wetenschappelijk Onderzoek - Vlaanderen FWO EOS Project no 30452698 '(MUSE-WINET) MUlti-Service WIreless NETwork'. The associate editor coordinating the review of this letter and approving it for publication was G. Chen. *(Corresponding author: Erica Debels.)*

The authors are with the Department of Telecommunication and Information Processing (TELIN), Ghent University, 9000 Gent, Belgium (e-mail: erica.debels@ugent.be; marc.moeneclaey@ugent.be).

Digital Object Identifier 10.1109/LCOMM.2020.3046104

TABLE I
SYMBOL DESCRIPTION TABLE

$V_{\mathrm{RF,TX}}$	TX rms voltage	ρ	current splitting factor
V_{RF}	RX rms voltage	f_{rect}	rectifier characteristic
v_{ID}	voltage at ID	w_{rect}	rectifier noise
P_{EH}	harvested power	w_{ADC}	quantization noise
v_{rect}	rectifier output	w_{ID}	total noise at ID
γh	channel gain	$\mathcal{A}_M$	M-ASK constellation

During the kth symbol interval $(kT, kT+T)$, an RF voltage $v_{\mathrm{RF,TX}}(t)$ is applied to the TX antenna, with

$$v_{\mathrm{RF,TX}}(t) = \sqrt{2}|a(k)|V_{\mathrm{RF,TX}}\cos(2\pi f_c t + \angle a(k)), \quad (1)$$

where $|a(k)|$ and $\angle a(k)$ denote the magnitude and the phase of $a(k)$; the rms value of $v_{\mathrm{RF,TX}}(t)$ in the considered symbol interval equals $|a(k)|V_{\mathrm{RF,TX}}$, giving rise to a long-term rms value equal to $V_{\mathrm{RF,TX}}$. The complex-valued channel gain is represented as γh, where $-20\log(\gamma)$ denotes the pathloss in dB, and h is the normalized fading gain. We assume that $h = |h|e^{j\angle h}$ is constant over a block of K symbol intervals; the magnitude $|h|$ has a Nakagami-m distribution[1] [15] with $\mathbb{E}[|h|^2] = 1$, and $\angle h$ arbitrarily distributed in the interval $[0, 2\pi)$. The RF voltage received at the rectifier input for $t \in (kT, kT+T)$ is represented as[2]

$$v_{\mathrm{RF,RX}}(t) = \sqrt{2}V_{\mathrm{RF}}|h||a(k)|\cos(2\pi f_c t + \theta(k)), \quad (2)$$

where $V_{\mathrm{RF}} = \gamma V_{\mathrm{RF,TX}}$ and $\theta(k) = \angle a(k) + \angle h$. The rms values of the rectifier input signal $v_{\mathrm{RF,RX}}(t)$ in the considered symbol interval, in the K-symbol block characterized by the fading gain h, and in the long term are given by $|h||a(k)|V_{\mathrm{RF}}$, $|h|V_{\mathrm{RF}}$, and V_{RF}, respectively. The corresponding rectifier output signal $v_{\mathrm{rect}}(t)$ is decomposed as

$$v_{\mathrm{rect}}(t) = f_{\mathrm{rect}}\left(|h||a(k)|V_{\mathrm{RF}}\right) + w_{\mathrm{rect}}(t), \quad (3)$$

where $w_{\mathrm{rect}}(t)$ is the zero-mean Gaussian rectifier output noise, with variance σ^2_{rect}. The function $f_{\mathrm{rect}}(A)$ is referred to as the rectifier characteristic, which expresses the DC component of the rectifier output voltage in terms of the rms value A of a sinusoidal input signal. We consider the simple rectifier circuit from Fig. 2, of which we determine the characteristic $f_{\mathrm{rect}}(A)$ in section III. The resistive load R_{L} in Fig. 2 represents the parallel connection of the EH part (load R_{L}/ρ) and the ID part (load $R_{\mathrm{L}}/(1-\rho)$) of the receiver, which draw currents $\rho\frac{v_{\mathrm{rect}}}{R_{\mathrm{L}}}$ and $(1-\rho)\frac{v_{\mathrm{rect}}}{R_{\mathrm{L}}}$, respectively, where ρ denotes the current splitting factor. The average harvested power equals $P_{\mathrm{EH}} = \eta_{\mathrm{EH}}\rho\mathbb{E}[f^2_{\mathrm{rect}}\left(V_{\mathrm{RF}}|h||a(k)|\right)]/R_{\mathrm{L}}$, where the expectation is with respect to $a(k)$ and $|h|$ and $\eta_{\mathrm{EH}} \in (0,1)$ denotes the EH efficiency. The current drawn by the ID part is fed to a sampler and analog-to-digital converter (ADC), which results in the voltage $v_{\mathrm{ID}}(k)$ which is used for information decoding; this voltage is decomposed as

$$v_{\mathrm{ID}}(k) = (1-\rho)f_{\mathrm{rect}}\left(|h||a(k)|V_{\mathrm{RF}}\right) + w_{\mathrm{ID}}(k), \quad (4)$$

[1]For integer m, the Nakagami-m distribution also applies to the case of an m-antenna TX applying maximum-ratio transmission on identically distributed Rayleigh-fading channels [15].

[2]The rectifier input noise is neglected, compared to the much larger rectifier output noise [5].

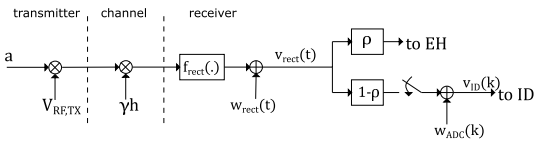

Fig. 1. Model for the IIE-RX.

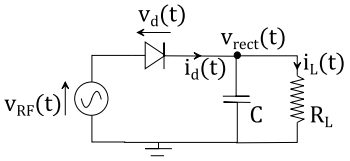

Fig. 2. Simple rectifier circuit.

where $w_{\mathrm{ID}}(k) = (1-\rho)w_{\mathrm{rect}}(kT) + w_{\mathrm{ADC}}(k)$, with $w_{\mathrm{ADC}}(k)$ the zero-mean Gaussian noise with variance σ^2_{ADC}, introduced by the ADC. The variance of $w_{\mathrm{ID}}(k)$ equals $\sigma^2_{\mathrm{ID}} = (1-\rho)^2\sigma^2_{\mathrm{rect}} + \sigma^2_{\mathrm{ADC}}$.

As (4) indicates that $v_{\mathrm{ID}}(k)$ does not depend on the phase of the data symbol $a(k)$, we restrict our attention to a biased M-ASK constellation, consisting of real-valued non-negative constellation points, hence allowing non-coherent detection. The normalized constellation is defined as $\mathcal{A}_M = \{\alpha_l, l = 0, \ldots, M-1\}$, with $\alpha_l = l\Delta$ and $\Delta = \left(\frac{1}{6}(M-1)(2M-1)\right)^{-\frac{1}{2}}$.

III. RECTIFIER CHARACTERISTIC

Let us determine the characteristic $f_{\mathrm{rect}}(A)$ of the rectifier from Fig. 2. The rectifier output voltage $v_{\mathrm{rect}}(t)$ is determined by the differential equation

$$C\frac{\mathrm{d}v_{\mathrm{rect}}}{\mathrm{d}t} + \frac{v_{\mathrm{rect}}}{R_{\mathrm{L}}} = I_{\mathrm{s}} \cdot \left(e^{\frac{1}{nV_{\mathrm{th}}}(v_{\mathrm{RF}} - v_{\mathrm{rect}})} - 1\right), \quad (5)$$

where V_{th} is the thermal voltage, and the diode is characterized by the reverse saturation current I_{s} and ideality factor n. Considering a sinusoidal input signal $v_{\mathrm{RF}}(t) = \sqrt{2}A\cos(2\pi f_0 t)$ with rms value A, $v_{\mathrm{rect}}(t)$ is periodic with period $1/f_0$ in steady-state operation. Assuming that $2\pi f_0 R_L C \gg 1$, the ripple in $v_{\mathrm{rect}}(t)$ can be safely neglected. Averaging both sides of (5) over an interval of duration $1/f_0$ yields, after rearranging,

$$\left(\frac{V_{\mathrm{DC}}}{I_{\mathrm{s}}R_{\mathrm{L}}} + 1\right)e^{\frac{V_{\mathrm{DC}}}{nV_{\mathrm{th}}}} = I_0\left(\frac{\sqrt{2}A}{nV_{\mathrm{th}}}\right). \quad (6)$$

where V_{DC} is the DC component of the rectifier output voltage $v_{\mathrm{rect}}(t)$, and $I_0(x) = \frac{1}{2\pi}\int_{-\pi}^{\pi} e^{x\cos(\theta)}\mathrm{d}\theta$ is the zero-order modified Bessel function of the first kind. The dependence of V_{DC} on A is denoted $V_{\mathrm{DC}} = f_{\mathrm{rect}}(A)$. The rectifier characteristic $f_{\mathrm{rect}}(A)$ resulting from (6) is shown in Fig. 3, for typical parameter values $I_{\mathrm{s}} = 5\mu\mathrm{A}$, $n = 1.05$, $R_{\mathrm{L}} = 1600\Omega$ and $V_{\mathrm{th}} = 25.85\mathrm{mV}$ [11]. For small A, $f_{\mathrm{rect}}(A)$ is quadratic in A: approximating each side of (6) by a truncated Taylor series expansion around $V_{\mathrm{DC}} = A = 0$ containing only the two nonzero lowest-order terms, we obtain

$$f_{\mathrm{rect}}(A) = \frac{1}{2}\left(\frac{1}{R_{\mathrm{L}}I_{\mathrm{s}}} + \frac{1}{nV_{\mathrm{th}}}\right)^{-1} \cdot \left(\frac{A}{nV_{\mathrm{th}}}\right)^2 \quad (7)$$

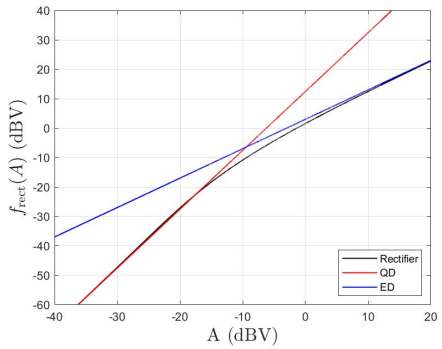

Fig. 3. Rectifier characteristics, showing DC output voltage versus rms input voltage.

for small A. For large A, the rectifier can be approximated by an ED [6], with:

$$f_{\rm rect}(A) = \sqrt{2}A. \tag{8}$$

Fig. 3 confirms that the rectifier characteristic approaches the characteristics of the QD (7) and of the ED (8) for small A (say, $A < -10$ dBV) and large A (say, $A > -10$ dBV), respectively.

The above analysis method can be extended to more involved circuit models (e.g., taking impedance matching circuit and parasitic elements into account), but the resulting rectifier characteristic is similar to the one from Fig. 3, with quadratic behavior for small A and linear behavior for large A [14].

IV. BER Analysis

We consider the transmission of uncoded symbols from the biased M-ASK constellation $\mathcal{A}_M$. This constellation gets distorted by the rectifier: the signal component in $v_{\rm ID}(k)$ corresponding to $a(k) = \alpha_l$ is denoted as $S_l = (1-\rho) f_{\rm rect}(|h|\alpha_l V_{\rm RF})$. As the noise is added *after* the rectifier, maximum-likelihood (ML) detection of $a(k)$ minimizes $|v_{\rm ID}(k) - S_l|$ over l: the ML decision on $a(k)$ yields $\widehat{a}(k) = \alpha_l$ when $v_{\rm ID}(k)$ is in the decision interval $\mathcal{D}_l = (d_l, d_{l+1})$ associated with S_l. The decision thresholds are located halfway between the signal components S_l, i.e., $d_l = \frac{1}{2}(S_{l-1}+S_l)$ for $l = 1, \ldots, M-1$, $d_0 = -\infty$, and $d_M = +\infty$. Hence, to perform ML detection, the receiver must know the distorted constellation $\{S_0, \ldots, S_{M-1}\}$; this constellation can be estimated from the transmission of pilot symbols sent during part of the considered fading block.

For given $|h|$, the BER is given by ([16], Ch. 4.3)

$$\text{BER} = \frac{1}{M}\frac{1}{\log_2(M)} \sum_{i,j=0}^{M-1} n_{i,j} P_{i,j} \tag{9}$$

where $n_{i,j}$ is the number of bits in which α_i and α_j differ, and $P_{i,j}$ is the probability that α_i is detected when α_j is transmitted. It can be verified that $P_{i,j} = P_{i,j}^{(1)} - P_{i,j}^{(2)}$, where $P_{0,j}^{(2)} = P_{M-1,j}^{(2)} = 0$, and $P_{i,j}^{(u)} = Q\left(\frac{D_{i,j}^{(u)}}{2\sigma_{\rm ID}}\right)$ for ($u = 2$, $i = 1, .., M-2$) and for ($u = 1$, $i = 0, \ldots, M-1$}); $Q(x)$ denotes the complement of the cumulative standard Gaussian distribution function, and $D_{i,j}^{(u)} = |2S_j - S_i - S_{i-(-1)^u \text{sgn}(\alpha_j - \alpha_i)}|$, with $u = 1, 2$, represents the distances between S_j and the boundaries of the decision interval $\mathcal{D}_i$. Because of the nonlinear nature of $f_{\rm rect}(A)$, the BER cannot be expressed as a function of the instantaneous signal-to-noise ratio (SNR), $|h|^2 V_{\rm RF}^2/\sigma_{\rm ID}^2$. When $f_{\rm rect}(A)$ is proportional to A^β, the BER (9) is a function of $|h|^\beta V_{\rm RF}^\beta/\sigma_{\rm ID}$; for the ED and the QD, we have $\beta = 1$ and $\beta = 2$, respectively.

Obtaining the average BER, denoted $\text{BER}_{\rm avg}$, requires taking the expectation of $P_{i,j}$ over the channel magnitude $|h|$, for all $i = 0, \ldots M-1$ and $j = 0, \ldots, M-1$, with $i \neq j$. For the actual rectifier characteristic $f_{\rm rect}(\cdot)$ resulting from (6), these expectations cannot be obtained analytically. However, for small $\sigma_{\rm ID}$, the average BER will be dominated by the large BER values that occur during deep fades, i.e., for small signal values at the input of the rectifier. Assuming that $f_{\rm rect}(A) \approx c_0 \cdot A^\beta$ for small A, $D_{i,j}^{(u)}$ is well approximated by $\gamma_{i,j}^{(u)} \left(\sqrt{x} V_{\rm RF}\right)^\beta$ for $u = 1, 2$, where $x = |h|^2$ and $\gamma_{i,j}^{(u)} = (1-\rho)c_0 |2\alpha_j^\beta - \alpha_i^\beta - \alpha_{i-(-1)^u \text{sgn}(\alpha_j - \alpha_i)}^\beta|$.

In the case of Nakagami-m fading with $\mathbb{E}[|h|^2] = 1$, $x = |h|^2$ we have the probability density function [15]

$$p_X(x) = \frac{m^m}{\Gamma(m)} x^{m-1} \exp(-mx) \tag{10}$$

with $\Gamma(m)$ denoting the Gamma function. The expectation of $P_{i,j}^{(u)}$ then becomes

$$\mathbb{E}\left[P_{i,j}^{(u)}\right] = \int_0^\infty Q\left(\frac{\gamma_{i,j}^{(u)} \left(\sqrt{x} V_{\rm RF}\right)^\beta}{2\sigma_{\rm ID}}\right) p_X(x) \text{d}x \tag{11}$$

For small $\sigma_{\rm ID}$, the first factor in the integrand rapidly decays to zero with increasing x, so that the second factor can safely be approximated as $p_X(x) = \frac{m^m}{\Gamma(m)} x^{m-1}$ for small x. The expectation of $P_{i,j}$ for small $\sigma_{\rm ID}$ then reduces to

$$\mathbb{E}[P_{i,j}] = 2^{2m/\beta} \frac{m^m}{\Gamma(m)} D(m, \beta, i, j) \left(\frac{\sigma_{\rm ID}^{2/\beta}}{V_{\rm RF}^2}\right)^m \tag{12}$$

where $D(m, \beta, i, j) = B(m, \beta, i, j) I(m, \beta)$ with $I(m, \beta) = \int_0^\infty Q\left(y^{\beta/2}\right) y^{m-1} \text{d}y$, $B(m, \beta, i, j) = \left(\gamma_{i,j}^{(1)}\right)^{-2m/\beta}$ for $i \in \{0, M-1\}$, and $B(m, \beta, i, j) = \left(\gamma_{i,j}^{(1)}\right)^{-2m/\beta} - \left(\gamma_{i,j}^{(2)}\right)^{-2m/\beta}$ otherwise.

Replacing in (9) $P_{i,j}$ by $\mathbb{E}[P_{i,j}]$ from (12) yields the low-noise approximation of $\text{BER}_{\rm avg}$:

$$\text{BER}_{\rm avg} \approx C_{\mathcal{A}_M}(m, \beta) \cdot \left(\frac{\sigma_{\rm ID}^{2/\beta}}{V_{\rm RF}^2}\right)^m, \tag{13}$$

with $C_{\mathcal{A}_M}(m, \beta) = \frac{m^m}{\Gamma(m)} \frac{1}{M} \frac{1}{\log_2(M)} \cdot \sum_{i,j=0}^{M-1} n_{i,j} D(m, \beta, i, j)$. It follows from (13) that, for small $\sigma_{\rm ID}$, $\text{BER}_{\rm avg}$ is inversely proportional to $V_{\rm RF}^{2m}$ and proportional to $\sigma_{\rm ID}^{2m/\beta}$. For the rectifier from Fig. 2, its small-signal quadratic approximation, and the ED, we have $\beta = 2$, $\beta = 2$, and $\beta = 1$, respectively, indicating a performance advantage of the ED over the rectifier for small $\sigma_{\rm ID}$.

The above analysis holds for arbitrary non-negative-valued constellation points (e.g., $\alpha_l = \sqrt{(l+1)\Delta}$ as in [7]) since

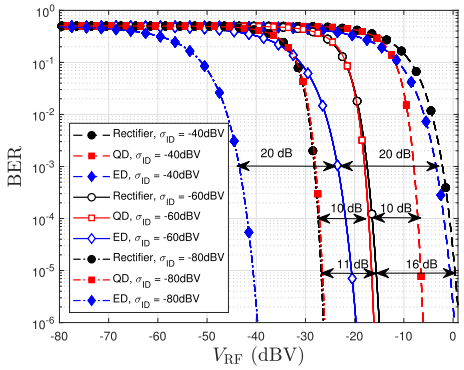

Fig. 4. Conditional BER ($|h| = 1$) versus V_{RF} (2-ASK).

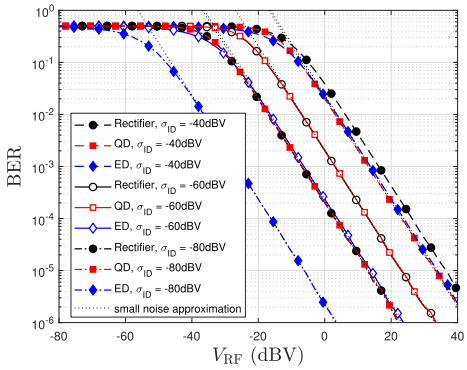

Fig. 5. Average BER on a Nakagami-m fading channel versus V_{RF} (2-ASK, $m = 1$).

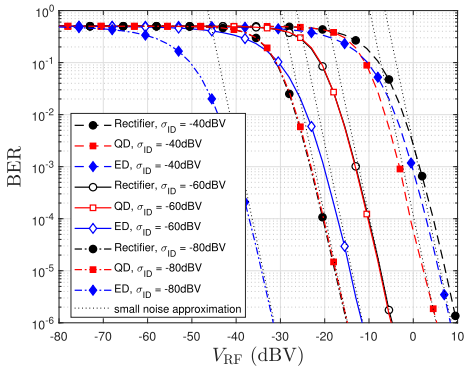

Fig. 6. Average BER on a Nakagami-m fading channel versus V_{RF} (2-ASK, $m = 4$).

only the functions $D(m, \beta, i, j)$ in (12) depend on the constellation points. The application of a nonlinear function to $v_{\mathrm{ID}}(k)$ (as in [6], where the compensation yields equi-spaced decision thresholds) does not affect the BER.

V. Numerical Results

Assuming that the noise variances σ^2_{rect} and σ^2_{ADC} are related by[3] $\sigma^2_{\mathrm{ADC}} = 10^{-4}\sigma^2_{\mathrm{rect}}$, we set the current splitting ratio as $\rho = 0.954$. This way, the resulting SNR at the input of the ADC and the harvested power are both only about 0.2 dB below their maximum values, achieved at $\rho = 0$ and $\rho = 1$, respectively [13]. For $\sigma_{\mathrm{ID}} \in \{-80\ \mathrm{dBV}, -60\ \mathrm{dBV}, -40\ \mathrm{dBV}\}$, we simulate the dependence on V_{RF} of the conditional BER with $|h| = 1$ and the long-term average BER on a Nakagami-m fading channel with $\mathbb{E}[|h|^2] = 1$, for the rectifier circuit from Fig. 2, the ED (8), and the QD (7).

Fig. 4 shows the conditional BER (9), in the case of uncoded biased 2-ASK transmission. For given σ_{ID} and increasing V_{RF}, or equivalently a decreasing BER, the penalty of the rectifier compared to the QD gets larger, whereas the BER curves for the rectifier and the ED approach each other. When σ_{ID} drops by 20 dB, the BER curves related to the ED and the QD shift to the left by 20 dB and 10 dB, respectively. This is in line with the analysis of the conditional BER in section IV; as this property holds irrespective of $|h|$, this behavior will also be observed for $\mathrm{BER}_{\mathrm{avg}}$ (see Figs. 5-7). In Fig. 4, the leftward shift of the BER curve associated with the rectifier from Fig. 2 is between 10 dB and 20 dB; for low V_{RF}, the shift is closer to 10 dB, whereas for high V_{RF}, the shift is closer to 20 dB, because the rectifier tends to behave like a QD and a ED, respectively.

Fig. 5 displays $\mathrm{BER}_{\mathrm{avg}}$ for a Nakagami-m block-fading channel with $m = 1$ (which corresponds with Rayleigh fading) and uncoded biased 2-ASK. For all three rectifier characteristics, for a given σ_{ID} and for low $\mathrm{BER}_{\mathrm{avg}}$, $\mathrm{BER}_{\mathrm{avg}}$ drops by a factor close to 10 when V_{RF} is increased by 10 dB. The BER for the rectifier virtually coincides with the BER for the quadratic detector when $\sigma_{\mathrm{ID}} \in \{-80\ \mathrm{dBV}, -60\ \mathrm{dBV}\}$, even when the average operating point of the rectifier is far outside the quadratic region (e.g., up to $V_{\mathrm{RF}} \approx 30$ dBV for $\sigma_{\mathrm{ID}} = -60$ dBV). These observations are consistent with the low-noise expression (13) of $\mathrm{BER}_{\mathrm{avg}}$, which is also shown in Fig. 6. For $\sigma_{\mathrm{ID}} = -40$ dBV, the average BER for the actual rectifier is worse than for the SD; this is because σ_{ID} is too large for the small-noise assumption leading to (13) to be accurate.

In Fig. 6, $\mathrm{BER}_{\mathrm{avg}}$ is shown for the Nakagami parameter $m = 4$ and uncoded biased 2-ASK. At low $\mathrm{BER}_{\mathrm{avg}}$, $\mathrm{BER}_{\mathrm{avg}}$ now drops by a factor close to 10 when V_{RF} is increased by 2.5 dB, i.e., the slope of the BER curves is increased by a factor 4 compared to the case $m = 1$. Hence, the BER performance improves with increasing m, which is explained by $p_X(x)$ from (10) becoming more concentrated around $x = 1$; at BER $= 10^{-6}$ and $\sigma_{\mathrm{ID}} \in \{-80\ \mathrm{dBV}, -60\ \mathrm{dBV}\}$, a considerable gain of about 37 dB in terms of V_{RF} is achieved for the rectifier, when comparing $m = 4$ to $m = 1$. For $\sigma_{\mathrm{ID}} \in \{-80\ \mathrm{dBV}, -60\ \mathrm{dBV}\}$, the rectifier and the QD yield virtually the same BER. As was the case for $m = 1$, a larger deviation between these BER curves occurs for $\sigma_{\mathrm{ID}} = -40$ dBV.

Fig. 7 shows $\mathrm{BER}_{\mathrm{avg}}$, for a Nakagami-$m$ block-fading channel with $m = 4$, and uncoded biased 8-ASK transmission. Similar conclusions regarding the slopes of the curves and their relative positions can be drawn as for Fig. 6. Compared to 2-ASK, 8-ASK requires a larger V_{RF} to achieve a given $\mathrm{BER}_{\mathrm{avg}}$, because of the smaller distance between constellation points.

Fig. 8 shows the average harvested power (for $\eta_{\mathrm{EH}} = 60\%$ [5]) versus V_{RF} on the Nakagami-m fading channels with $m = 1$ and $m = 4$, for 2-ASK. The harvested power does not

[3]As explained in [5], the quantization noise is typically much smaller than the rectifier output noise.

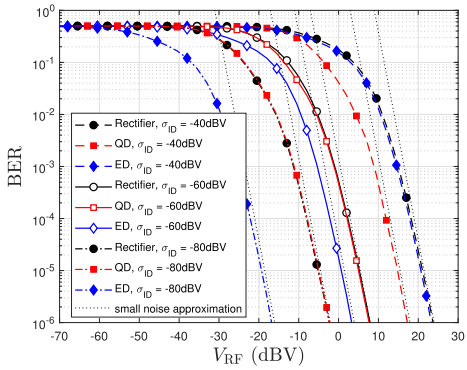

Fig. 7. Average BER on a Nakagami-m fading channel versus V_{RF} (8-ASK, $m = 4$).

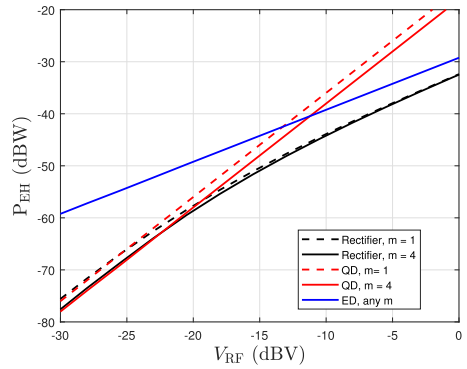

Fig. 8. Average $\mathrm{P_{EH}}$ (with $\eta_{\mathrm{EH}} = 0.6$) on a Nakagami-m fading channel, versus V_{RF} (2-ASK).

depend on m for the ED and only weakly depends on m for the rectifier and the QD. Unlike the error performance of the ID, the harvested powers resulting from the rectifier and the QD (the ED) are very close when the average operating point of the former is in the quadratic (the linear) region.

VI. Conclusion

We have investigated the BER of the ID for SWIPT with an IIE-RX, for the uncoded transmission of biased ASK on a Nakagami-m fading channel, and presented an analytical expression for the resulting BER in the small-noise regime. Although the characteristics of the rectifier and the QD differ considerably for larger input signals, their small-noise BER curves nearly coincide, even when the average operating point of the rectifier is outside the quadratic region. This behavior does not occur for a fixed channel gain, where the BER of the rectifier is closer to the BER of the ED when the rectifier operating point is outside the quadratic region.

References

[1] L. R. Varshney, "Transporting information and energy simultaneously," in *Proc. IEEE Int. Symp. Inf. Theory*, Toronto, ON, Canada, Jul. 2008, pp. 1612–1616.

[2] R. Zhang and C. K. Ho, "MIMO broadcasting for simultaneous wireless information and power transfer," *IEEE Trans. Wireless Commun.*, vol. 12, no. 5, pp. 1989–2001, May 2013.

[3] T. D. Ponnimbaduge Perera, D. N. K. Jayakody, S. K. Sharma, xS. Chatzinotas, and J. Li, "Simultaneous wireless information and power transfer (SWIPT): Recent advances and future challenges," *IEEE Commun. Surveys Tuts.*, vol. 20, no. 1, pp. 264–302, 1st Quart., 2018.

[4] R. Zhang, R. G. Maunder, and L. Hanzo, "Wireless information and power transfer: From scientific hypothesis to engineering practice," *IEEE Commun. Mag.*, vol. 53, no. 8, pp. 99–105, Aug. 2015.

[5] X. Zhou, R. Zhang, and C. K. Ho, "Wireless information and power transfer: Architecture design and rate-energy tradeoff," *IEEE Trans. Commun.*, vol. 61, no. 11, pp. 4754–4767, Nov. 2013.

[6] S. Claessens, N. Pan, M. Rajabi, D. Schreurs, and S. Pollin, "Enhanced biased ASK modulation performance for SWIPT with AWGN channel and dual-purpose hardware," *IEEE Trans. Microw. Theory Techn.*, vol. 66, no. 7, pp. 3478–3486, Jul. 2018.

[7] R. Zhang, L.-L. Yang, and L. Hanzo, "Energy pattern aided simultaneous wireless information and power transfer," *IEEE J. Sel. Areas Commun.*, vol. 33, no. 8, pp. 1492–1504, Aug. 2015.

[8] E. Goudeli, C. Psomas, and I. Krikidis, "An integrated SWIPT receiver using non-coherent detection schemes," in *Proc. IEEE Global Commun. Conf. (GLOBECOM)*, Abu Dhabi, United Arab Emirates, Dec. 2018, pp. 1–7, doi: 10.1109/GLOCOM.2018.8647432.

[9] Y. Al-Eryani, "Exact performance of wireless-powered communications with maximum ratio combining," *Wireless Pers. Commun.*, vol. 108, pp. 1665–1675, Oct. 2019.

[10] H. K. Sahu, P. R. Sahu, and J. Mishra, "ABEP of SSK with SWIPT at relay and generalised selection combining at the destination over Rayleigh fading," in *Proc. Nat. Conf. Commun. (NCC)*, Kharagpur, India, 2020, pp. 1–6.

[11] B. Clerckx and E. Bayguzina, "Waveform design for wireless power transfer," *IEEE Trans. Signal Process.*, vol. 64, no. 23, pp. 6313–6328, Dec. 2016.

[12] R. Morsi, V. Jamali, D. W. K. Ng, and R. Schober, "On the capacity of SWIPT systems with a nonlinear energy harvesting circuit," in *Proc. IEEE Int. Conf. Commun. (ICC)*, Kansas City, MO, USA, May 2018, pp. 20–24.

[13] E. Debels and M. Moeneclaey, "Optimized linear precoding for biased 2-ASK modulation in multi-user SWIPT with integrated receiver," in *Proc. IEEE 91st Veh. Technol. Conf. (VTC-Spring)*, Antwerp, Belgium, May 2020, pp. 1–5.

[14] R. G. Harrison, "Full nonlinear analysis of detector circuits using ritz-Galerkin theory," in *IEEE MTT-S Int. Microw. Symp. Dig.*, Albuquerque, NM, USA, 1992, pp. 267–270.

[15] M. Nakagami, "The m-distribution—A general formula of intensity distribution of rapid fading," in *Statistical Methods in Radio Wave Propagation*. Oxford, U.K.: Pergamon Press, 1960, pp. 3–36.

[16] J. G. Proakis and M. Masoud, *Digital Communications*, 5th ed. New York, NY, USA: McGraw-Hill, 2008.